https://doi.org/10.5194/egusphere-2026-4120
Preprint. Discussion started: 7 August 2026

ENSO simulation in the coupled Korean Integrated Model

Sae-Rim Yeo [1], Myung-Seo Koo [1], Eunjeong Lee [1], Kyung-Hee Seol[1]

[1]Korea Institute of Atmospheric Prediction Systems (KIAPS), Seoul, 07071, South Korea

Correspondence to: Myung-Seo Koo (mskoo@kiaps.org)

Abstract. This study presents a comprehensive evaluation of the El Niño–Southern Oscillation (ENSO) simulation characteristics in the newly established coupled Korea Integrated Model (coupled KIM), which is designed for extended-range prediction. To robustly diagnose ENSO behavior, a 171-year coupled simulation was conducted and systematically evaluated against eight CMIP6 models that share the Nucleus for European Modelling of the Ocean (NEMO) as their oceanic component. Benchmarking the CLIVAR 2020 ENSO metrics framework, we evaluate diverse aspects of ENSO, including its spatial pattern, intensity, skewness, seasonality, and teleconnections, within the context of the tropical Pacific mean state. The coupled KIM exhibits moderate to above-average performance across most key metrics. Notably, the model successfully mitigates the common systematic bias of an excessive westward extension of the ENSO sea surface temperature (SST) pattern. This improvement is linked to a warmer eastern Pacific mean state compared to other CMIP6 models. However, this warm bias leads to a weak zonal SST gradient and a relatively deeper-than-normal thermocline, which consequently underestimates the overall ENSO intensity. Furthermore, this eastern Pacific warm bias undergoes pronounced seasonal expansion during January–February, intimately synchronized with an amplified double ITCZ bias. This seasonal coupling further flattens the simulated ENSO seasonality, although the ratio of ENSO amplitude between winter and spring remains one of the most realistic among the evaluated models. The model also demonstrates outstanding skill in reproducing ENSO skewness, which is plausibly attributed to recent advancements in the vertical mixing processes of the NEMO component. Additionally, the coupled KIM realistically captures tropical precipitation anomalies and their teleconnection patterns, including the extratropical atmospheric responses in the Northern Hemisphere. These findings validate the current developmental trajectory of the coupled KIM and highlight its robust potential for reliable extended-range forecasting.

1 Introduction

The Korea Institute of Atmospheric Prediction Systems (KIAPS) was established with the strategic mandate to develop a state-of-the-art national numerical weather prediction (NWP) system. During its first project phase (2010–2019), KIAPS successfully developed the Korean Integrated Model (KIM), which has served as the operational forecasting system of the Korea Meteorological Administration since 2020 (Hong et al., 2018). Building on this operational foundation, KIAPS is pursuing the development of a next-generation modeling system during its second project phase (2020–2026). One of the primary goals of this effort is to establish a seamless prediction system capable of spanning short- to extended-range timescales, expending predictability up to approximately one month (Lee et al., 2024; Yeo et al., 2026). To support this forecast range extension, which critically depends on the realistic simulation of evolving boundary conditions, a coupled modeling system based on KIM has been developed (Koo et al., 2025a), hereafter referred to as the coupled KIM. This comprehensive system advances existing land-surface processes and dynamically couples the atmosphere with state-of-the-art ocean, sea ice, wave, and river-routing components. Detailed configurations of the coupled KIM are provided in Sect. 2.

The latest version of the coupled KIM has been rigorously optimized, achieving medium-range forecast skill comparable to that of the existing atmosphere-only configuration. However, demonstrating skill at the medium-range does not automatically guarantee stability or fidelity for longer integration periods. To robustly evaluate the performance of the coupled KIM, long-term historical simulations equivalent to the Coupled Model Intercomparison Project (CMIP) standards are required (Eyring et al., 2016; Durack et al., 2025). Such extended integrations are necessary to scrutinize the model's climatological mean state and internal variability, avoiding the aliasing of decadal noise and uncovering systematic biases that only emerge over time. These foundational assessments underpin the further development of skillful extended-range prediction. In this context, this study evaluates the performance of the coupled KIM through long-term integrations, with a primary focus on its ability to simulate the El Niño–Southern Oscillation (ENSO). As the dominant mode of coupled interannual variability in the tropical Pacific, ENSO provides a physically meaningful benchmark for assessing the fidelity of atmosphere-ocean coupling, the delicate balance of large-scale thermodynamic and dynamic feedback processes, and the overall stability of coupled models. Furthermore, ENSO serves as the primary pacemaker for global climate variability on subseasonal-to-seasonal timescales, modulating extratropical weather patterns through complex atmospheric teleconnections (e.g., Alexander et al., 2002; Martineau et al., 2021). Therefore, the accurate simulation of ENSO's amplitude, spatial structure, and temporal evolution is an essential prerequisite for achieving the goals of seamless prediction.

Given the central role of ENSO in coupled model evaluation, the Pacific Regional Panel of the Climate and Ocean: Variability, Predictability, and Change (CLIVAR) project developed an objective ENSO metric package. This package was designed to facilitate standardized, reproducible, and comprehensive diagnostics across diverse climate models (Planton et al., 2021). In this study, we adopt this framework as a baseline to design ENSO diagnostics for the coupled KIM. To provide a deeper contextual evaluation, the results are systematically compared with a subset of CMIP6 models that share the Nucleus for European Modelling of the Ocean (NEMO) as their ocean component, as does the coupled KIM. This specific comparative approach is strategically advantageous; by constraining the diversity of ocean component, it becomes easier to identify features and biases unique to the coupled KIM's atmospheric physics and air-sea flux formulations, as well as to isolate systematic errors commonly shared across NEMO-based coupled models. This methodology effectively contextualizes the performance of the coupled KIM within the current generation for Earth system models, highlighting both its competitive strengths and area requiring further parametrization refinement.

The remainder of this paper is organized as follows. Sect. 2 describes the architecture of the coupled KIM system, the experimental design for the long-term simulations, the selected CMIP6 models, and observational datasets used for validation. Sect. 3 presents a detailed evaluation of the ENSO characteristics simulated by the coupled KIM in comparison with the

https://doi.org/10.5194/egusphere-2026-4120
Preprint. Discussion started: 7 August 2026

reference models. Specifically, we examine the spatial patterns, intensity, skewness, seasonality, and global teleconnections associated with ENSO variability. Finally, Sect. 4 summarizes the overall performance of the coupled KIM, discusses the physical mechanisms underlying the identified biases, and offers main implications for future model development.

2 Data and Methodology

2.1 Brief introduction to the coupled KIM

KIM employs a spectral-element, nonhydrostatic dynamical core on a cubed-sphere grid (Choi and Hong, 2016) and incorporates a state-of-the-art physics suite designed for operational medium-range forecasting (Hong et al., 2018). The model configuration and physical processes employed in this study are largely based on Lee et al. (2024), with several recent advancements in physical parameterization (Baek and Kim, 2024; Han, 2025; Koo and Hong, 2025; Kim, 2025). To extend the capability of KIM toward extended-range prediction, a fully coupled framework incorporating interactive ocean, sea ice, wave, and land surface components has been developed for operational applications (Koo et al., 2025). Within this system, NEMO (Madec et al., 2024), together with the Sea Ice Modelling Integrated Initiative (SI^3) (Vancoppenolle et al., 2023), is used to represent oceanic dynamics and physics, and the WAVEWATCH III (WW3) (WW3 Development Group, 2019) model is additionally coupled to better represent ocean wave effects. Furthermore, the existing Noah land surface model (LSM) (Ek et al., 2003) is replaced with the Noah with multiparameterization (Noah-MP) LSM (Niu et al., 2011) to simulate more complex biophysical and hydrological process over land.

The interactions among these components are managed through a coupling framework based on the Model Coupling Toolkit (MCT; Larson et al., 2005), with coupling fields exchanged at an hourly interval. In this configuration, KIM provides atmospheric forcing to the other components, including near-surface (first model level) wind, temperature, and specific humidity, as well as radiative fluxes, sea-level pressure, and freshwater fluxes from precipitation and snowfall. In return, NEMO supplies lower boundary conditions to KIM, such as sea surface temperature (SST) and sea ice surface temperature, enabling fully interactive air–sea and air–ice feedbacks. The coupling architecture is designed such that the outputs from SI^3 and WW3 are routed through NEMO, providing a consolidated set of oceanic fluxes to KIM. Recently, this coupled KIM configuration was successfully employed to investigate how air-sea interactions improve the simulation of synoptic patterns (Kwak et al., 2025) and to assess the impact of sea ice simulation fidelity on extended-range forecast skill (Park et al., 2024).

2.2 Long-term integration with the coupled KIM

Long-term integrations with the coupled KIM are conducted following the standard CMIP6 historical simulation protocol (Eyring et al., 2016). The atmospheric component (i.e., KIM) is configured with a NE090 and 91 vertical levels. Here, NE090 denotes the number of spectral elements along each face of the cubed-sphere grid, corresponding to a horizontal

https://doi.org/10.5194/egusphere-2026-4120
Preprint. Discussion started: 7 August 2026

resolution of approximately 50 km. The oceanic component (i.e., NEMO/SI^3) employs the extended ORCA (eORCA) grid with a nominal horizontal resolution of 0.25° and 75 unevenly spaced vertical levels.

The external forcing fields are prescribed following the CMIP6 historical protocol. Specifically, total solar irradiance, carbon dioxide (CO_2), ozone (O_3), and other well-mixed greenhouse gases are applied using the CMIP6 forcing datasets, with time-varying forcing from 1850 to 2014. Due to compatibility constraints between the CMIP6 aerosol forcing formulation and the operational KIM physics package, aerosol forcing is prescribed using the Monitoring Atmospheric Composition and Climate (MACC) dataset currently employed in KIM operations. To prevent long-term drift in the sea surface salinity (SSS) and ensure the stability of the meridional overturning circulation, SSS restoring term is applied in NEMO (Griffies et al., 2009). This configuration ensures numerical stability and physical consistency for long-term coupled integrations while retaining a realistic representation of atmospheric composition.

To initialize the atmospheric and oceanic states of the coupled KIM, the European Centre for Medium-range Weather Forecasts (ECMWF) Global Reanalysis version 5 (ERA5; Hersbach et al., 2020) and the Ocean Reanalysis System 5 (ORAS5; Zuo et al., 2019) datasets are used, respectively. For sea ice thickness initialization, data from the Global Ice Ocean Modeling and Assimilation System (GIOMAS) and the Pan-Arctic Ice Ocean Modeling and Assimilation System (PIOMAS) (Zhang and Rothrock, 2003) are utilized. Due to the unavailability of reanalysis data for 1 January 1850, the conditions from 1 January 1979 were used as a proxy. Consequently, the pre-industrial control run, typically required by the CMIP6 protocol, was omitted in this study. While this introduces an initial discontinuity between the 1850 and forcing and 1979 states, preliminary sensitivity tests confirmed that this reanalysis-based initialization strategy yielded robust performance, with negligible differences compared to simulations that include a standard spin-up period. Using these external forcing datasets and initial conditions, a 171-year simulation was conducted with the coupled KIM, spanning the period from 1850 to 2020. For the period after 2015, the 2014 external forcing data were repeatedly applied as a constant background.

To rigorously account for the model's dynamic adjustment to the 1850 radiative forcing and to eliminate any potential 'initialization shock' arising from the use of the 1979 state, the first 100 years of the simulation are treated as a spin-up period and are deliberately excluded from the evaluation. Consequently, all ENSO analyses presented in this study are based on the remaining period after 1951, ensuring that the assessed climatology and internal variability are robust and free from initial transient drifts. Further details are given in the next sub-Sect..

2.3 Validation

The primary objective of this study is to identify and evaluate the ENSO characteristics simulated by the coupled KIM. Accordingly, SST is used as the principal variable for model validation. As an observational reference, we employ the National Oceanic and Atmospheric Administration (NOAA) Optimum Interpolation Sea Surface Temperature (OISST) dataset (Huang et al., 2021), which is provided at a horizontal resolution of 0.25° and is available from September 1981 onward and the observational reference period for validation is set to 1982-2020 (39 years).

https://doi.org/10.5194/egusphere-2026-4120
Preprint. Discussion started: 7 August 2026

In addition to SST, zonal wind stress is used as a key variable for ENSO evaluation and is validated against the National Center for Environmental Prediction (NCEP)/Department of Energy (DOE) Reanalysis 2 dataset (Kalnay et al., 2018). Precipitation is validated using the Global Precipitation Climatology Project (GPCP) dataset (Adler et al., 2018). Because the 1° GPCP product is available only from October 1996 onward, precipitation-related validation is performed for the period 1997–2020 (24 years). For completeness, additional analyses using the lower-resolution 2.5° GPCP dataset over the full 1982–2020 period were conducted, and no substantial differences in the results were found. The reference geopotential height variable is derived from the ERA5 data.

To place the ENSO characteristics of the coupled KIM in a broader modeling context, intercomparisons are performed with historical simulations from eight CMIP6 coupled models (Eyring et al., 2016) that employ NEMO as their ocean component. Information on these models is summarized in Table 1. We only analyzed the first realization (r1i1p1f1) of each model. The CMIP6 models are analyzed over the final 39 years of their historical simulations (1976–2014). For consistency, all model outputs and observational reanalysis datasets are regridded to a common 1° horizontal resolution prior to analysis. Note that the coupled KIM employs finer horizontal resolutions in both its atmospheric and oceanic components than any of the other models compared in this study (Table 1). The implications of this difference and its potential impact on resolving coupled feedback processes will be discussed in the final Sect..

Table 1. Summary of model configurations for NEMO-coupled CMIP6 models and the coupled KIM

Model name/Country	Atmospheric model	NEMO version	Resolution (Atm/Ocn)	DOI
CanESM5/Canada	CanAM5	v3.4	2.8x2.8, 49levs/1	https://doi.org/10.22033/ESGF/CMIP6.3610
CMCC-CM2-SR5/Italy	CAM5.3	v3.6	0.9x1.25, 30levs/1	https://doi.org/10.22033/ESGF/CMIP6.3825
CNRM-CM6-1/France	ARPEGE6.3	v3.6	1x1, 91levs/1	https://doi.org/10.22033/ESGF/CMIP6.4066
EC-Earth3/EU	IFS	v3.6	1.9x1.9, 91levs/1	https://doi.org/10.22033/ESGF/CMIP6.4700
HadGEM3-GC31-LL/UK	MetUM-HadGEM3-GA7.1	v3.6	1.875×1.25, 85levs/1	https://doi.org/10.22033/ESGF/CMIP6.6109
IPSL-CM6A-LR/France	LMDZ6	v3.6	2.5×1.259, 79levs/1	https://doi.org/10.22033/ESGF/CMIP6.5195
NESM3/China	ECHAMv6.3	v3.4	1.9x1.9, 47levs/1	https://doi.org/10.22033/ESGF/CMIP6.8769
UKESM1-0-LL/UK	MetUM-HadGEM3-GA7.1	v3.6	1.875×1.25, 85levs/1	https://doi.org/10.22033/ESGF/CMIP6.6113
Coupled KIM/Korea	KIM	v4.0	0.5x0.5, 91levs/0.25	

https://doi.org/10.5194/egusphere-2026-4120
Preprint. Discussion started: 7 August 2026

As briefly noted in the previous sub-Sect., the temporal framework of the long-term simulation of coupled KIM does not exactly follow that of the CMIP6 historical experiment, owing to the use of reanalysis-based initial conditions and the absence of a pre-industrial control integration. Therefore, instead of adopting the final 36 years of the simulation, the validation period was selected based on both the stability of the long-term integration and its consistency with the observational SST records.

Figure 1a shows the global-mean, annual-mean net radiative flux at the top of the atmosphere (TOA), defined as incoming solar radiation minus the sum of outgoing longwave and reflected shortwave radiation. The net radiative flux converges toward zero after more than 50 years of integration, indicating that the coupled system has reached a satisfactorily equilibrated energetic state. During the final three decades of the simulation (post-1990), however, the net radiative flux becomes slightly positive. Figure 1b presents the annual-mean SST averaged over 60°S–60°N from the coupled KIM simulation. Consistent with the positive TOA net radiation flux, the simulated SST exhibits a pronounced warming trend after 1990. To identify the model period most comparable to the observed SST climatology, multiple 39-year segments from the coupled KIM simulation were compared against the OISST record for 1982–2020. This comparison showed that the simulation period 1952–1990 provides the closest agreement with the observed mean state (Fig. 1b).

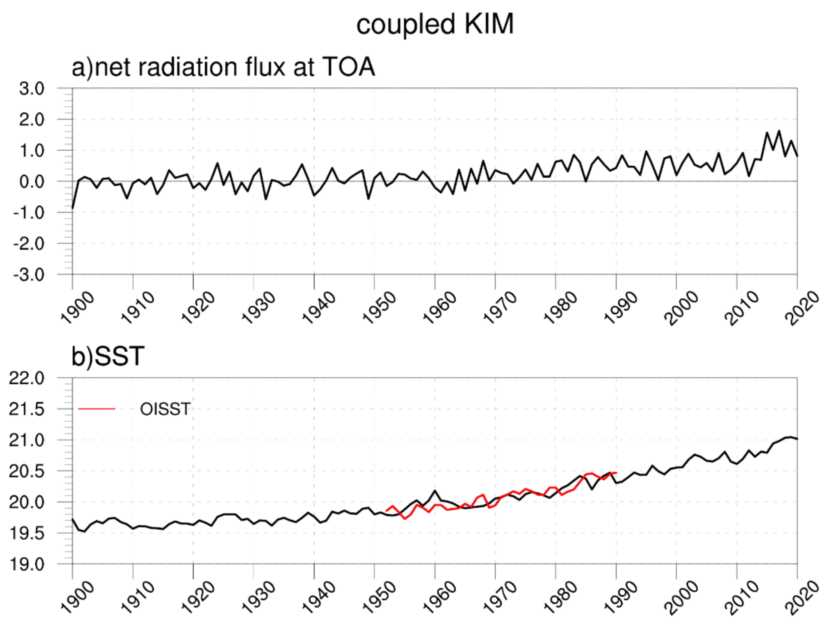

Figure 1: a) Annual-mean, global-mean net radiative flux at the top of the atmosphere (TOA) and b) annual-mean sea surface temperature (SST) averaged over 60°S–60°N in the coupled KIM simulation over the period 1900–2020. The TOA net radiative flux is defined as incoming solar radiation minus outgoing longwave and reflected shortwave radiation. The observed OISST time series for 1982–2020 is overlaid in red in (b).

https://doi.org/10.5194/egusphere-2026-4120
Preprint. Discussion started: 7 August 2026

This temporal discrepancy may arise from differences in the model's transient response to external forcing relative to the real climate system, including differences in adjustment timescale and effective climate sensitivity. It may also partly reflect the fact that the long-term coupled simulation has not yet been fully optimized for historical transient forcing—a common challenge when adapting an NWP-focused model for extended climate integrations. Since this study represents an initial attempt to perform long-term climate simulations with a model primarily developed for NWP applications, further optimization will be addressed in future work. Therefore, the 1952–1990 period of coupled KIM simulation—during which both the SST climatology and the global energy balance are most consistent with observations—was selected as the validation period. This choice is further motivated by the fact that key aspects of coupled atmosphere–ocean variability, including ENSO, are highly sensitive to the background mean state. Evaluating the model during the period in which the simulated SST climatology is most consistent with observations allows for a more meaningful assessment of the model's coupled behavior while minimizing the influence of mean-state bias.

3 ENSO simulation in coupled KIM

3.1 Pattern

We begin our evaluation of ENSO simulation in the coupled KIM by examining its ability to reproduce the spatial patterns of ENSO. Figures 2a–c present the SST anomaly patterns regressed onto the Niño3.4 index (SST anomaly averaged over 5°S–5°N, 170°W–120°W) for December, derived from the OISST, the multi-model composite of the eight CMIP6 reference models, and the coupled KIM simulation, respectively. To isolate the robust boreal winter ENSO signal, the December SST anomalies are smoothed using a 5-month triangular-weighted moving average. Unless otherwise stated, 'December' refers to 5-month triangular-weighted moving average centered on December throughout this study.

Compared to the OISST observation, the CMIP6 models tend to simulate ENSO-related SST anomalies that extend excessively into the western Pacific (Fig. 2b). In contrast, the SST anomalies in the eastern Pacific are generally underestimated. In addition, the observed cold SST anomalies over the northwestern Pacific are poorly reproduced by the CMIP6 composite, and the ENSO-related SST anomalies tend to extend too far into the southeastern Pacific. The coupled KIM exhibits a bias pattern broadly similar to that of the CMIP6 models, including the overestimation in the southeastern Pacific and a westward extension of the ENSO pattern relative to observation (Fig. 2c). However, the cold SST anomalies over the northwestern Pacific are more realistically simulated in the coupled KIM. More importantly, the degree of the artificial westward extension of ENSO-related SST anomalies is weaker in the coupled KIM than in the CMIP6 composite.

https://doi.org/10.5194/egusphere-2026-4120
Preprint. Discussion started: 7 August 2026

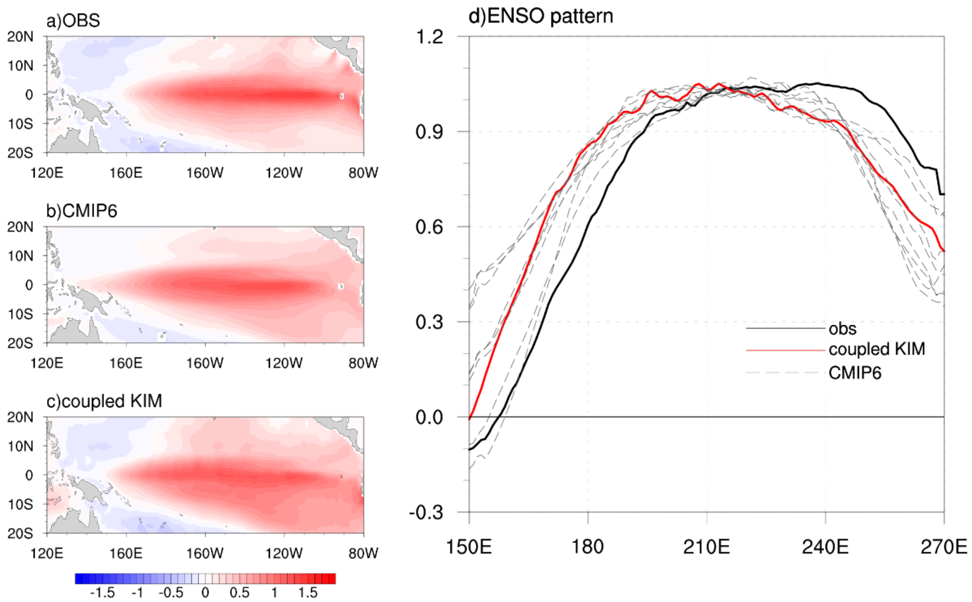

Figure 2: SST anomaly patterns regressed onto the Niño3.4 index from (a) OISST, (b) the multi-model mean of the eight CMIP6 models, and (c) the coupled KIM. (d) Zonal distribution of ENSO-related SST anomalies averaged over 5°S–5°N for observations (black solid line), the individual CMIP6 models (gray dashed lines), and the coupled KIM (red solid line).

The characteristics of the simulated ENSO patterns are more clearly illustrated in Fig. 2d, which shows the zonal structure of ENSO-related SST anomalies averaged over the tropical Pacific (5°S–5°N). Consistent with the spatial maps, all models share a common tendency to overestimate SST anomalies in the western Pacific and underestimate them in the eastern Pacific. Nevertheless, compared with the CMIP6 reference models, the magnitude of both the westward overextension and the eastern Pacific underestimation is relatively smaller in the coupled KIM.

The excessive westward extension of ENSO-related SST anomalies is a well-documented, pervasive bias across CMIP models, not merely confined to those utilizing the NEMO ocean (e.g., Collins et al., 2010; Kim and Yu, 2012; Jiang et al., 2021). Jiang et al. (2021) demonstrated that this bias is closely linked to errors in the simulated mean tropical SST, particularly an overly strong and westward-displaced cold tongue (CT) in the equatorial Pacific. This CT bias steepens the mean zonal SST gradient in the equatorial western–central Pacific, which in turn strengthens the zonal advection feedback, favoring the unrealistically westward extension of the ENSO SST pattern.

To elucidate how the mean SST state in the coupled KIM influences its ENSO pattern simulation – particularly the relatively weaker westward extension compared to other models – Fig. 3a presents the December climatology of the tropical (5°S–5°N) mean SST for the observation, the coupled KIM, and the eight CMIP6 models. Consistent with the previous studies, all models simulate a westward displaced CT, which leads to an enhanced zonal SST gradient around the central-western Pacific. While the coupled KIM also exhibits this westward-displaced CT, its intensity differs from those from most other

https://doi.org/10.5194/egusphere-2026-4120
Preprint. Discussion started: 7 August 2026

models. In most CMIP6 models, the CT is excessively strong, manifesting as overly cold bias. In contrast, the coupled KIM, together with CanESM5 and EC-Earth3, simulates a weaker CT that is relatively warmer than observation. Overall, the coupled KIM simulates the CT intensity more realistically than most of the other models. This tropical Pacific mean SST structure in the coupled KIM, characterized by a weaker CT, leads to a relatively weaker zonal SST gradient across the central Pacific than in the other CMIP6 models. These features are clearly evident in Fig. 3b, which shows the zonal SST gradient averaged over the tropical central Pacific (5°S–5°N, 180°–220°E). The coupled KIM exhibits a relatively weak zonal SST gradient that is closer to observations. Note, although EC-Earth3 shows a strong warm bias extending from the CT region into the eastern Pacific, a warm bias is also present from the western Pacific onward, resulting in a zonal SST gradient over the central Pacific that is comparable to the observations.

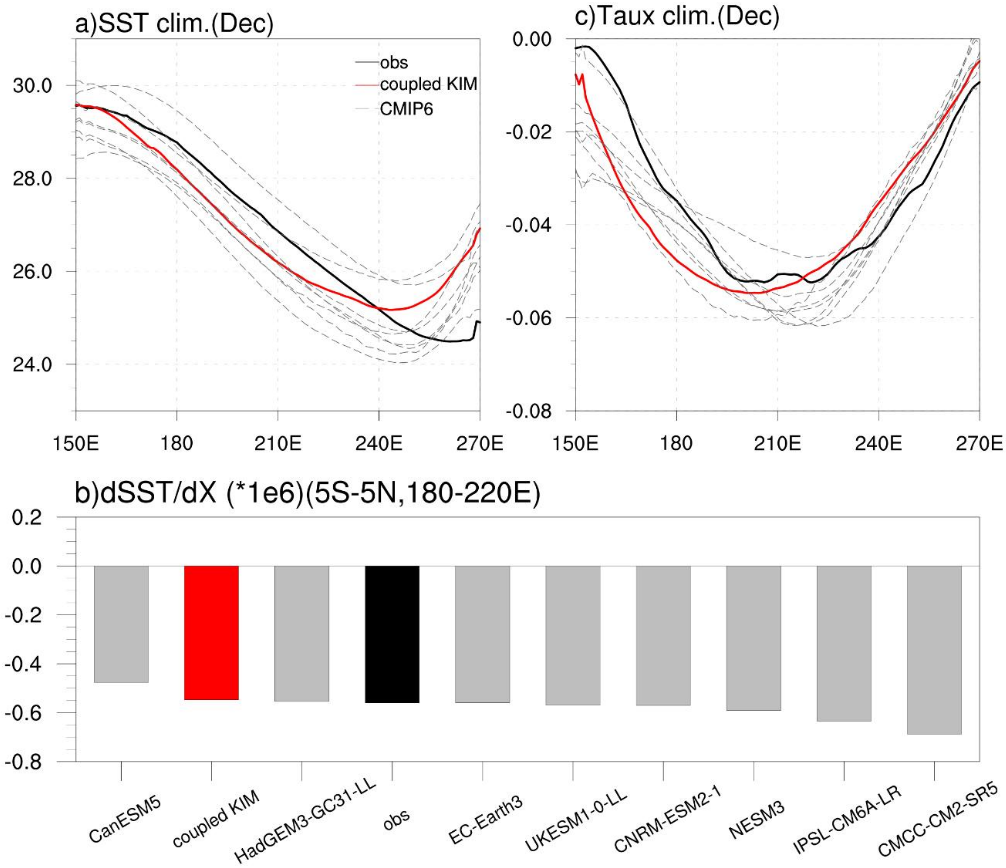

Figure 3: December climatology of tropical (5°S–5°N) zonal-mean (a) SST and (c) zonal wind stress for observations (black solid lines), the individual CMIP6 models (gray dashed lines), and the coupled KIM (red solid line). (b) Zonal SST gradient averaged over the tropical central Pacific (5°S–5°N, 180°–220°E) for observations (black bar), the individual CMIP6 models (gray bars), and the coupled KIM (red bar).

https://doi.org/10.5194/egusphere-2026-4120
Preprint. Discussion started: 7 August 2026

This background SST structure is dynamically coupled to the mean zonal wind stress. The climatology of the tropical mean zonal wind stress shown in Fig. 3c displays that most models simulate intensified easterly wind stress over the regions from the western to the central Pacific (150°–230°E) compared to the observations. While the coupled KIM also exhibits excessively strong easterly wind stress over the western Pacific, it shows weaker easterly wind stress over the central Pacific around 210°E. This is physically consistent with its reduced zonal SST gradient in that region associated with the warm bias around the CT. This zonally non-uniform mean state structure acts to moderate the zonal advection feedback identified by Jiang et al. (2021), thereby reducing the tendency for ENSO-related SST anomalies to extend excessively westward.

3.2 Intensity and skewness

The next diagnostic metrics examined are ENSO intensity and skewness. ENSO intensity is evaluated using the standard deviation of the December Niño3.4 index, following the CLIVAR 2020 metric (Fig. 4a). While various factors influence the simulation of ENSO intensity (e.g., Kim et al., 2014), from a background mean state perspective, the primary drivers are the zonal advection feedback governed by the zonal temperature gradient, and the thermocline feedback through vertical mixing of subsurface temperature by the mean upwelling over the eastern Pacific (An and Jin, 2001; Guilyardi, 2006). Consistent with this framework, the coupled KIM, which exhibits a weak zonal temperature gradient, simulates one of the weaker ENSO intensities, whereas models with a stronger gradient, such as IPSL-CM6A-LR and CMCC-CM2-SR5, show the strong ENSO intensity (Figs. 3b and 4a). Furthermore, a shallower thermocline in the eastern Pacific is known to enhance the thermocline feedback, thereby increasing ENSO amplitude. However, most CMIP6 models exhibit a warm bias in the far eastern Pacific (Fig. 3a), which is primarily attributed to weak coastal upwelling. This suppressed upwelling leads to an anomalously deep thermocline, that likely contributes to the weakening of ENSO intensity in these models. The ENSO amplitude shown in Fig. 4a thus appears to emerge from a complex interaction between zonal advection feedback and thermocline feedback. For the coupled KIM, the weaker intensity of the CT plays a favorable role in suppressing the westward extension of ENSO patterns, but it also leads to the weak ENSO intensity, indicating a somewhat negative impact on ENSO intensity.

https://doi.org/10.5194/egusphere-2026-4120
Preprint. Discussion started: 7 August 2026

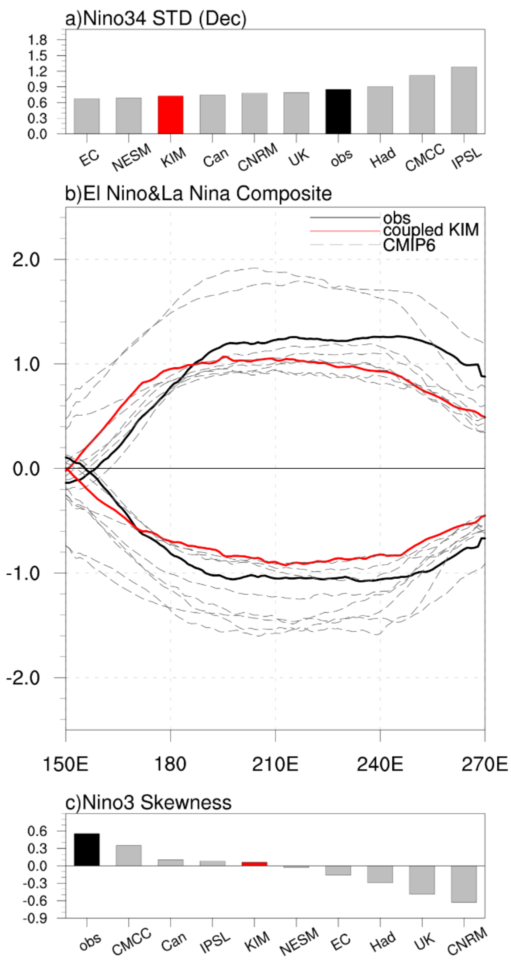

Figure 4: (a) Standard deviation and (c) skewness of the December Niño3.4 index for observation (black bar), the CMIP6 models (gray bars), and the coupled KIM (red bar). (b) Composite SST anomalies averaged over 5°S–5°N during El Niño and La Niña years for observation (black lines), the CMIP6 models (gray lines), and the coupled KIM (red lines).

To evaluate more detailed features of the ENSO intensity simulated by the models, El Niño and La Niña years are identified using a threshold of $\pm$0.75 standard deviations of the December Niño3.4 index. The composite tropical (5°S–5°N) mean SST anomaly patterns of these events for observation, the coupled KIM and CMIP6 models are shown in Fig. 4b. Excluding the notably strong El Niño amplitudes simulated by CMCC-CM2-SR5 and IPSL-CM6A-LR, most of the remaining models tend to underestimate El Niño intensity, while simulating La Niña intensity that is comparable to or stronger than observed. This asymmetry is directly linked to the skewness of ENSO intensity. Figure 4c shows the skewness averaged over the tropical eastern Pacific (5°S–5°N, 210°E–270°E). In the observations, ENSO exhibits a distinct positive skewness, reflecting the tendency for El Niño events to be stronger than La Niña events. Simulating this skewness remains a persistent challenge

https://doi.org/10.5194/egusphere-2026-4120
Preprint. Discussion started: 7 August 2026

in the coupled models, showing little systematic improvement across successive CMIP generations (Zhang and Sun 2014; Zhao and Sun 2022). Figure 4c reveals that five out of eight CMIP6 models exhibit negative skewness, indicating stronger La Niña than El Niño. Although CMCC-CM2-SR5 and IPSL-CM6A-LR simulate positive skewness, this arises from their unrealistically strong El Niño amplitudes, making their skewness physically inconsistent with observations. In contrast, the coupled KIM exhibits a weak but positive skewness (Fig. 4c). As shown in Fig. 4b, the coupled KIM simulates the weakest La Niña intensity among the models, while its El Niño intensity falls within the mid-range of the CMIP6 simulations. Consequently, although the magnitude of the skewness is smaller than observed, it represents one of the realistic ENSO asymmetry simulations among the evaluated models.

ENSO skewness is influenced by multiple factors, including nonlinear ocean–atmosphere coupling (Kang and Kug, 2002) and nonlinear vertical temperature advection (An and Jin, 2004). In this study, particular attention is given to the improved vertical diffusion scheme implemented in the NEMO component of the coupled KIM, introduced as part of ongoing physical process improvements. Specifically, this update acts to compensate for the limitations of local diffusion assumptions under unstable stratification by strengthening vertical mixing during convective conditions. As a result, the upper eastern tropical Pacific exhibits enhanced vertical homogenization, leading to a weakened near-surface vertical temperature gradient. At the same time, the update reduces vertical diffusivity below the mixed layer, thereby strengthening the stratification below the mixed layer and suppressing entrainment of cold subsurface water. Consequently, warm SST anomalies during El Niño events can persist longer and attain larger amplitudes, providing a plausible physical pathway for the enhanced El Niño intensity and the resulting positive ENSO skewness successfully simulated by the coupled KIM.

3.3 Seasonality

ENSO variability exhibits a strong phase locking to the seasonal cycle, with SST anomalies typically peaking during the boreal winter (November–January; NDJ) and reaching a minimum during boreal spring (March–May; MAM) (e.g., Neelin et al., 2000). To assess the ENSO seasonal phase-locking in the coupled KIM, Fig. 5a compares the standard deviation of the monthly Niño3.4 index from the coupled KIM with the observation and CMIP6 models. The observed ENSO evolution features a sharp growth during September–October (SO), reaching its peak during NDJ, followed by a sharp decay in February–March and minimal variability during the subsequent boreal spring and summer. In contrast, there are substantial inter-model spread in simulating ENSO seasonality, either showing little peak amplitude or peaking at the incorrect seasons. In particular, most models fail to capture the rapid growth toward the winter peak from SO to NDJ, resulting in a flattened seasonality rather than a distinct winter peak. The coupled KIM is no exception, sharing similar characteristics of seasonal evolution with other models.

https://doi.org/10.5194/egusphere-2026-4120
Preprint. Discussion started: 7 August 2026

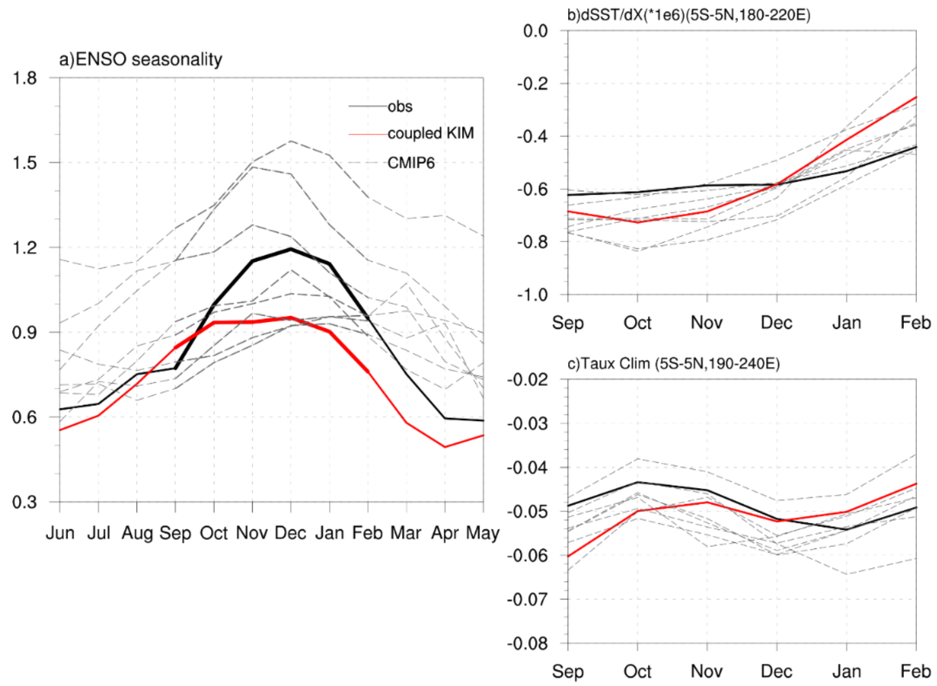

Figure 5: (a) Standard deviation of the monthly Niño3.4 index. The September–February period is highlighted with thicker lines. (b) monthly climatology of the zonal SST gradient averaged over 5°S–5°N, 180°–220°E, and (c) monthly climatology of zonal wind stress averaged over 5°S–5°N, 190°–240°E, from September to February. In all panels, observation, the individual CMIP6 models, and the coupled KIM are represented by black, gray, and red lines, respectively.

To diagnose the cause of the flat ENSO seasonality in these models, we further examine the monthly evolution of the mean state biases, focusing particularly on the period from September to February. Figures 5b and 5c show the time evolution of the monthly climatological zonal SST gradient and zonal wind stress averaged over the central tropical Pacific (5°S–5°N, 180°–220°E for SST and 190°–240°E for zonal wind stress) from September to February. As noted in Figs. 3a and 3b, the CT bias in many models leads to an overall overestimation of the zonal SST gradient in the central Pacific. However, a distinct seasonal feature of this bias is found; the overestimation is most pronounced during September–December, whereas the gradient becomes generally weaker than observations during January–February (JF) (Fig. 5b). Consistent with the SST gradient, the zonal wind stress exhibits an enhanced eastward stress bias from September to December, whereas in JF, this bias tends to be weaker in most models (Fig. 5c). These distinct seasonal structure in the tropical zonal SST gradient and zonal wind stress implies an enhanced zonal advection feedback during September-December, followed by a weakened feedback in JF. Consequently, these combined effects contribute to the ‘flattened’ ENSO seasonality, where the amplitude is spread from September to February rather than exhibiting a sharp peak in NDJ (Fig. 5a).

https://doi.org/10.5194/egusphere-2026-4120
Preprint. Discussion started: 7 August 2026

The coupled KIM demonstrates a substantial overestimation of the SST gradient and eastward zonal wind stress bias over the tropical central Pacific during SO. Furthermore, it shows a significant underestimation of these values during JF compared to other models as well as observation (Figs. 5b and 5c). To further investigate why the zonal SST gradient in the coupled KIM becomes particularly weak during JF, we examine the tropical mean state evolution in more detail. Figure 6 illustrates the zonal SST structure averaged over the tropics (10°S–5°N) from September to February, together with the corresponding precipitation patterns for observations, the coupled KIM, and their differences (coupled KIM minus observations). The coupled KIM simulates a westward extension of the eastern Pacific cold tongue (Fig. 6c), which is a systematic bias existing in many CMIP6 models (Fig. 3a). Concurrently, a pronounced warm bias is observed in the far eastern Pacific. A warm bias is also present over the western Pacific warm pool region. Close examination reveals that the bias patterns during JF differ notably from those observed in the preceding months. During JF, the eastern Pacific warm bias expands westward into the central Pacific, while the amplitude of the warm bias over the western Pacific and cold bias over the central Pacific weakens over time (Fig. 6c). As a result, the overall SST bias pattern shifts westward compared to the September-December period, leading to a marked weakening in the zonal SST gradient.

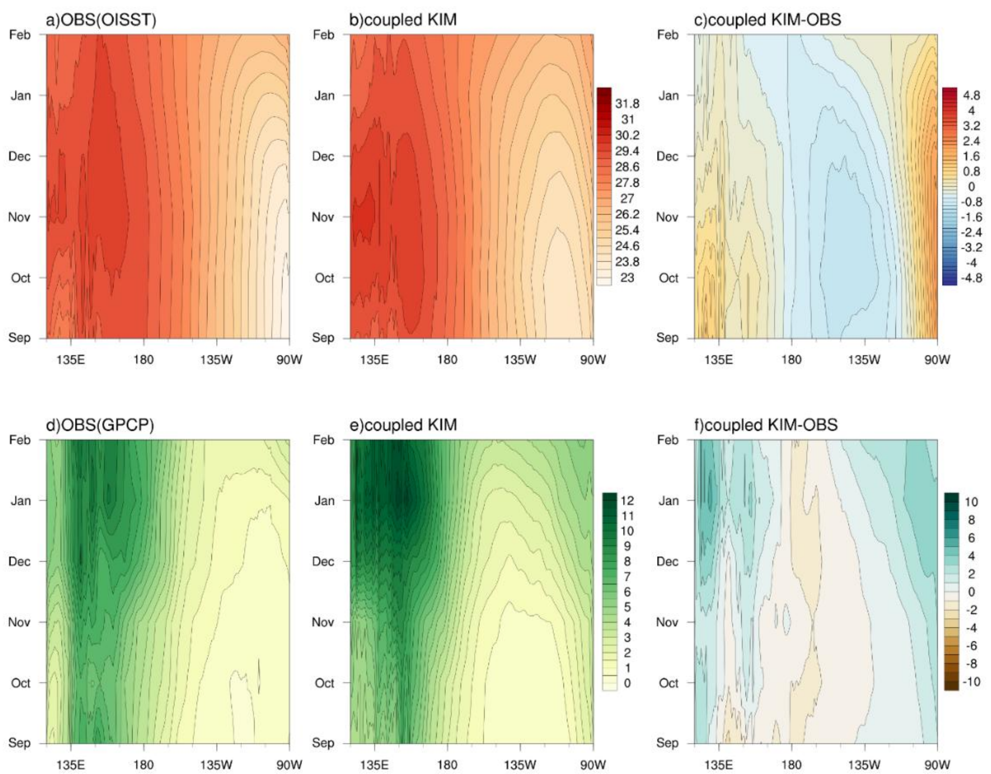

Figure 6: Zonal climatology of SST and precipitation averaged over 10°S–5°N from September to February for (a and d) observations, (b and e) the coupled KIM, and (c and f) the difference between the coupled KIM and observations.

https://doi.org/10.5194/egusphere-2026-4120
Preprint. Discussion started: 7 August 2026

The tropical Pacific is characterized by strong ocean-atmosphere coupling associated with the Walker circulation, in which warm SSTs over the western Pacific lead deep atmospheric convection, while compensating subsidence dominates over the eastern Pacific. Variations in this coupled system play a fundamental role in shaping both the mean state and variability of ENSO. To interpret the SST bias structure from an air-sea coupling perspective, the associated precipitation bias is examined along with the SST bias (Figs. 6d–f). The precipitation bias largely mirrors the SST bias pattern (Figs. 6c and 6f). In association with the westward displacement of the cold tongue, the climatological dry zone over the eastern Pacific is also shifted westward (Figs. 6d and 6e), leading to a dry bias over the central Pacific (Fig. 6f). At the same time, a positive precipitation bias is evident over the far eastern Pacific associated with the local warm SST bias. During JF, this wet bias extends westward into the central Pacific, accompanied by a corresponding expansion of the warm SST bias. A systematic overestimation of precipitation is also found over the western Pacific in association with the warm SST bias. In contrast to the far eastern Pacific, however, the positive precipitation bias extends eastward into the central Pacific (approximately 135°–160°E) during JF, while the warm SST bias over the western Pacific weakens. This behavior suggests that the enhanced precipitation bias acts to dampen the local warm SST bias, likely through increased cloud cover or enhanced evaporative cooling, implying a process in which atmospheric forcing exerts a thermodynamic feedback onto SST. As a consequence, the precipitation bias structure during JF acts to weaken the Walker circulation more effectively than implied by the SST bias alone. This enhanced weakening of the Walker circulation further reduces the zonal SST gradient in JF, providing a consistent dynamical explanation for the suppressed wintertime ENSO peak intensity in the coupled KIM.

A distinct feature of precipitation bias in coupled models is the so-called double Intertropical Convergence Zone (ITCZ) bias. This refers to the spurious simulation of excessive precipitation south of the equator in the eastern Pacific, in addition to the primary Northern Hemisphere ITCZ, often accompanied by an unrealistically zonally elongated South Pacific Convergence Zone (SPCZ). This double ITCZ problem is also recognized as a major factor contributing to the degraded simulation of ENSO seasonality (e.g., Zeng and Yu, 2007). To examine how the double ITCZ manifests in the coupled KIM and how it relates to both the ENSO seasonality and the overall tropical mean biases, Figs. 7a–d present the mean precipitation patterns for SO and JF from the observations and the coupled KIM. During SO, the coupled KIM overestimates precipitation associated with both the ITCZ and the SPCZ. However, no secondary convergence zone south of the equator is simulated, and thus a clear double ITCZ bias is not evident during this period (Figs. 7a and b). In contrast, during JF, the coupled KIM simulates an additional precipitation maximum near 5°S, indicative of a pronounced double ITCZ structure. This bias co-occurs with an excessive zonal SPCZ compared to the observations (Figs. 7c and 7d).

https://doi.org/10.5194/egusphere-2026-4120
Preprint. Discussion started: 7 August 2026

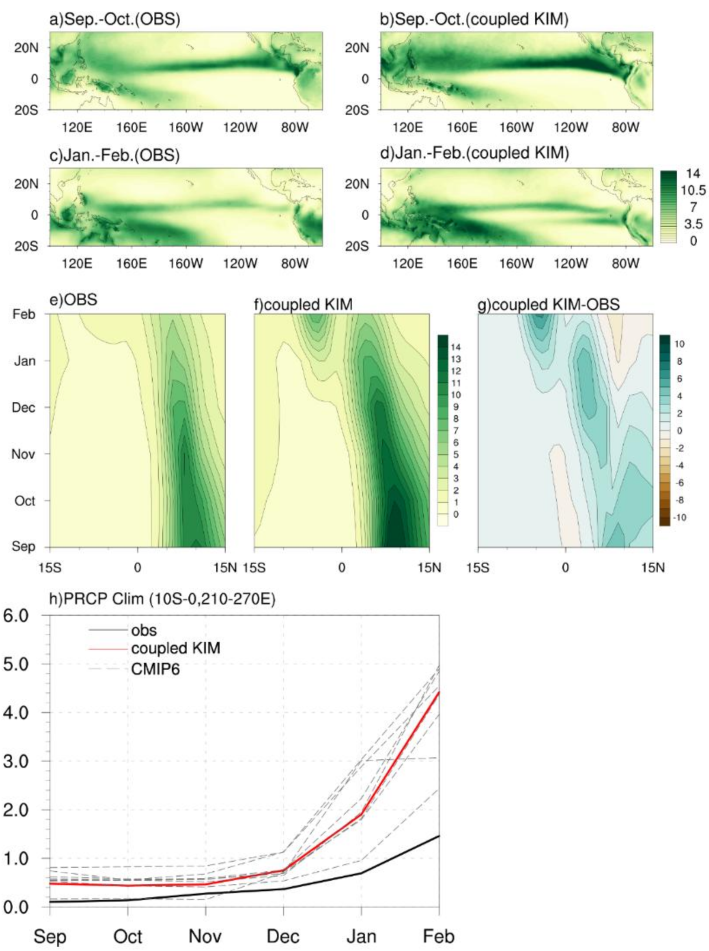

Figure 7: Climatological mean precipitation during (a and b) September–October and (c and d) January–February for observations (a and c) and the coupled KIM (b, d). (e–g) Meridional distribution of precipitation climatology averaged over 210°–270°E for (e) observations, (f) the coupled KIM, and (g) the coupled KIM minus observations. (h) Monthly climatology of precipitation averaged over 10°S–0°, 210°–270°E, from September to February for observations (black line), the individual CMIP6 models (gray lines), and the coupled KIM (red line).

This seasonal emergence of the double ITCZ bias is more clearly illustrated in the latitude–month cross section of precipitation averaged over the eastern Pacific (210°E–270°E) (Figs. 7e–g), which shows that the spurious southern convergence zone is most prominent during JF. To place the coupled KIM in a broader model context, precipitation averaged over the southeastern Pacific region where the double ITCZ typically appears (10°S–0°, 210°E–270°E) is compared among CMIP6 models from September to February (Fig. 7h). The results indicate that CMIP6 models also exhibit a strengthened double ITCZ bias during JF, with the coupled KIM showing a moderate bias relative to the CMIP6 models.

https://doi.org/10.5194/egusphere-2026-4120
Preprint. Discussion started: 7 August 2026

In summary, the westward extension of the eastern Pacific warm bias during JF in the coupled KIM acts to reduce ENSO amplitude, thereby contributing to a flattened seasonality of ENSO. This behavior appears to be closely linked to the strengthening of the double ITCZ during this period. An enhanced double ITCZ weakens the equatorial trade winds, which in turn suppresses upwelling in the eastern Pacific, reinforcing the warm SST bias. This warm bias further favors the persistence of the double ITCZ, forming a positive feedback loop. This limitation is not unique to the coupled KIM but is shared by many coupled models. Improving the representation of the double ITCZ is therefore expected to lead to broad improvements in ENSO simulation, including its amplitude, seasonality, and associated feedback processes.

3.4 Teleconnections

In the final sub-Sect., the ENSO teleconnection simulated by the coupled KIM is evaluated. In coupled prediction system, the realistic simulation of ENSO teleconnection is critical, as it directly influences extended-range predictability (e.g., Vitart et al., 2003). This study examines the basic features of ENSO teleconnection, which include the tropical precipitation response and the associated first-order Northern Hemisphere atmospheric response during December.

Figure 8a shows the tropical (5°S–5°N) averaged precipitation anomalies regressed onto the Niño3.4 index during December. Note that the observational results use the 1°–degree GPCP data available since 1997 (25 years; see Sect. 2), while the model results are based on 39 years. Analyses using the 2.5°–degree GPCP data over the full 39-year period produce qualitatively consistent results (not shown here). As shown in Fig. 8a, observations indicate that during the mature phase of El Niño, the center of tropical deep convection shifts eastward toward the dateline, accompanied by an anomalous suppression of convection over the tropical western Pacific. In contrast, most models, including the coupled KIM, systematically displace these anomalies westward relative to observations, accompanied by a significant inter-model spread in amplitude. This westward displacement is dynamically consistent with the tendency of coupled models to simulate ENSO SST anomaly patterns with an excessive westward extension (Fig. 2). Although the coupled KIM reproduces the main systematic biases common to the CMIP6 models, both the positional bias and amplitude errors are generally smaller than in most other models. In particular, the location and amplitude of the convective responses over the western Pacific and eastern Indian Ocean are simulated closer to observations in the coupled KIM than in the other models. This improved performance is primarily attributable to the relatively realistic simulation of the ENSO SST patterns in the coupled KIM, though it is likely further modulated by complex interactions involving vertical mixing processes, cloud-radiative feedbacks, and mean-state SST biases (e.g., Guilyardi et al., 2009), which warrant further investigation.

https://doi.org/10.5194/egusphere-2026-4120
Preprint. Discussion started: 7 August 2026

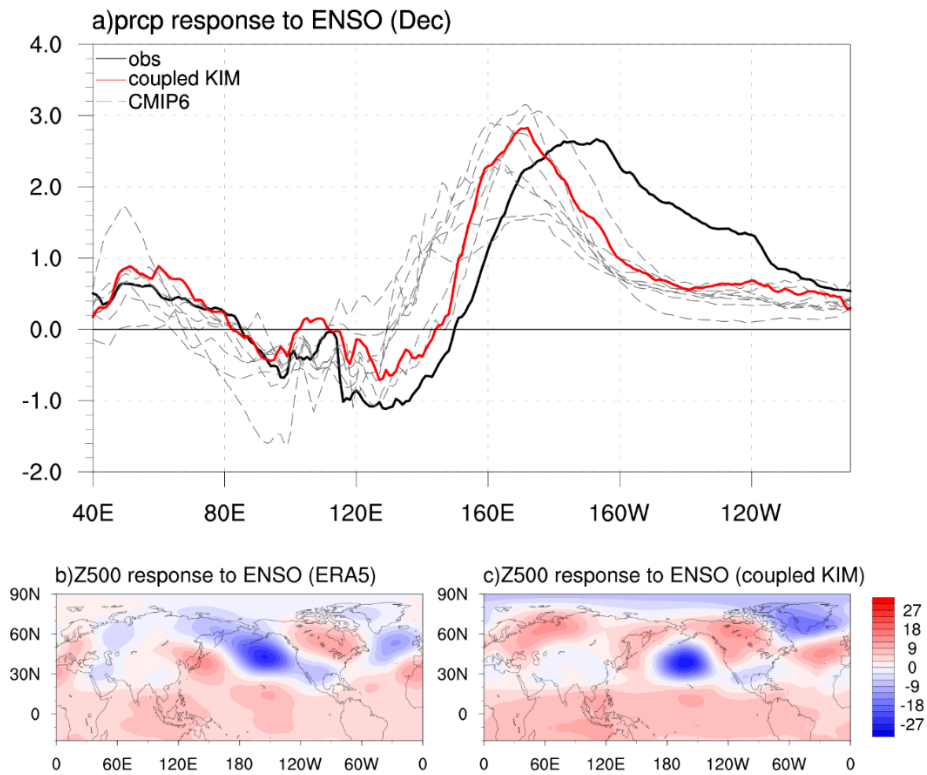

Figure 8: (a) Tropical (5°S–5°N) mean precipitation anomalies regressed onto the Niño3.4 index during December for observation (black line), the individual CMIP6 models (gray lines), and the coupled KIM (red line). (b) and (c) Z500 anomalies regressed onto the Niño3.4 index during December for ERA5 and the coupled KIM, respectively.

The diabatic heating associated with ENSO-related tropical precipitation anomalies excites a Rossby wave train that propagates into the extratropics. To evaluate the simulated atmospheric response, 500 hPa geopotential height (Z500) anomalies regressed onto the Nino3.4 index during December are examined. Figures 8b and 8c show the regressed Z500 anomaly patterns from ERA5 and the coupled KIM, respectively. In ERA5, El Niño triggers an alternating sequence of positive and negative Z500 anomalies in an arch-like shape from East Asia to the North Atlantic. In particular, the feature of a deepened Aleutian Low, followed by a ridge over North America and a downstream trough over the North Atlantic is characterized by the Pacific-North American (PNA) pattern (Wallace and Gutzler, 1981). The coupled KIM reproduces this sequence of large-scale atmospheric responses in a physically reasonable manner (Fig. 8c). However, the deficiencies remain in the simulation of teleconnection patterns over the Eurasian continent and the North Atlantic Ocean. These deficiencies are likely linked to biases in ENSO-related tropical heating and biases in the simulated extratropical mean state, particularly the upper-level jet, which can modify both the Rossby wave source and its propagation pathways.

https://doi.org/10.5194/egusphere-2026-4120
Preprint. Discussion started: 7 August 2026

4 Summary and discussion

This study presents a comprehensive evaluation of ENSO simulation characteristics in the coupled KIM, a system under development at KIAPS aimed at extending the prediction range. To this end, a long-term coupled simulation spanning 171 years was conducted, enabling a robust diagnosis of ENSO behavior. To provide a comprehensive assessment, we examined various aspects of ENSO, in terms of its spatial pattern, intensity, skewness, seasonality and teleconnections. For an objective evaluation, the coupled KIM, which employs NEMO as its oceanic component, was compared against eight CMIP6 models that also utilize NEMO.

Figure 9 presents a summary of these ENSO metrics in a portrait plot format, following the CLIVAR 2020 ENSO metric style. As discussed in the individual Sect., many aspects of ENSO simulation are closely tied to the representation of the tropical Pacific mean state, including SST, zonal wind stress, and precipitation. Accordingly, the first three columns of the portrait plot represent the root-mean-square error (RMSE) of these mean state variables relative to observations. Specifically, this refers to the RMSE calculated for the tropical (5°S–5°N) averaged zonal structure (150°E–270°E) during December. Subsequent columns summarize the ENSO-related metrics in the order discussed in this study: pattern, intensity, skewness, seasonality and teleconnection (precipitation and Z500). Specifically, the fidelity of the ENSO pattern is quantified by the RMSE of the regressed zonal SST structure relative to observations (Fig. 2d), while intensity and skewness are similarly evaluated based on their respective RMSEs (Figs. 4a and 4c). ENSO seasonality is assessed using the ratio of the standard deviation of the Niño3.4 index during NDJ to that during MAM, and this metric is also evaluated in terms of its RMSE from the observed value. For precipitation teleconnections, the metric is defined as the RMSE between the model-simulated and observed regression patterns shown in Fig. 8a. For Z500 teleconnections, spatial pattern correlations between the observed and simulated regressed Z500 anomalies are computed over the Northern Hemisphere extratropics (30°–80°N) and are likewise expressed as RMSE relative to the observed reference value (i.e., unity). To facilitate comparison across disparate metrics within a single figure, all values are standardized. In this representation, darker blue colors indicate models closer to the reference datasets, while darker red colors indicate larger deviations.

https://doi.org/10.5194/egusphere-2026-4120
Preprint. Discussion started: 7 August 2026

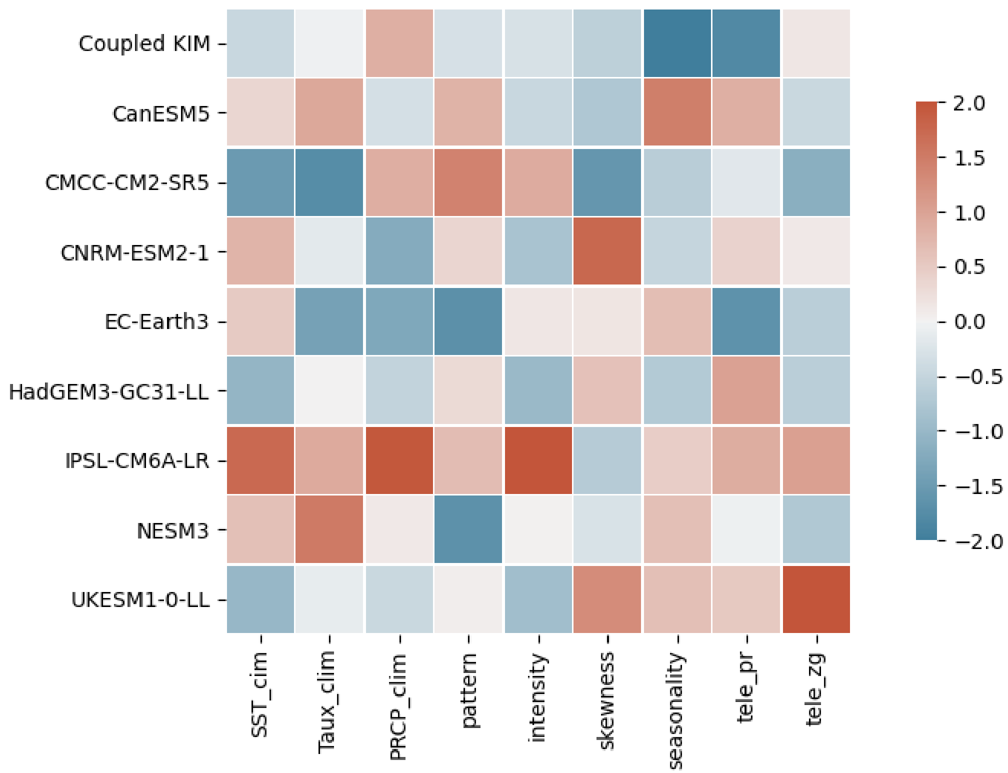

Figure 9: Portrait diagram summarizing ENSO metrics. Each metric is standardized by subtracting the column mean and dividing by the column standard deviation. Darker blue (red) colors indicate better (worse) agreement with the observational reference for a given metric. The metrics, in order, represent SST, zonal wind stress, and precipitation climatology; ENSO pattern; intensity; skewness; seasonality; and teleconnections in precipitation (pr) and geopotential height (zg).

As shown in Fig. 9, the coupled KIM exhibits moderate to above-average performance across most ENSO-related metrics. The coupled KIM simulates a warmer eastern Pacific compared to many other models that suffer from a 'too cold' CT bias. This bias acts to weaken the mean zonal SST gradient, which in turn helps mitigate the common model bias of an excessive westward extension of the ENSO SST pattern. However, this same mechanism also contributes to an underestimation of ENSO intensity. Notably, the eastern Pacific warm bias exhibits pronounced seasonal variability. During JF, the warm bias expands spatially in association with an enhanced double ITCZ bias. This further weakens the zonal SST gradient, leading to a reduced ENSO amplitude during the peak season and resulting in a flatter ENSO seasonality compared to observations. While, this behavior is common across many CMIP6 models, the ENSO seasonality in the coupled KIM, when evaluated by the ratio of ENSO intensity between NDJ and MAM, stands out as one of the most realistic among the models. The

https://doi.org/10.5194/egusphere-2026-4120
Preprint. Discussion started: 7 August 2026

coupled KIM also shows strength in simulating ENSO skewness. This strength is plausibly linked to enhancements in vertical mixing processes within the NEMO ocean component, which were introduced as part of recent physical process development and model optimization. ENSO teleconnection performance is also reasonable; the coupled KIM successfully reproduces the features of ENSO-related tropical precipitation anomalies and the associated extratropical atmospheric response. In addition to the metrics emphasized in this study, the CLIVAR 2020 ENSO framework also includes diagnostics of the ENSO life cycle, duration, and diversity. For these additional metrics, the coupled KIM exhibits generally reasonable performance compared to the CMIP6 models (not shown), further supporting the robustness of its ENSO simulation.

Several factors should be considered when interpreting these results. Although the comparison is restricted to CMIP6 models employing NEMO, differences remain in the NEMO versions (v3.4 or v3.6 in most CMIP6 models versus v4.0 in the coupled KIM, along with additional physical improvements), horizontal resolutions (with the coupled KIM utilizing a comparatively higher resolution; Table 1), and experimental design, as the long-term coupled simulation does not strictly follow the standard CMIP6 historical protocol. Model resolution, in particular, is known to exert a strong influence on ENSO simulation (Wengel et al., 2021; Liu et al., 2022). Despite these technical discrepancies, the results presented here remain highly meaningful because this study represents the first comprehensive evaluation of the coupled KIM—originally developed for extended-range prediction—in a long-term integration context. The analysis demonstrates that the coupled KIM already achieves ENSO simulation skill comparable to, or exceeding, that of many established CMIP6 coupled models, even in its current development stage. This validates the current developmental trajectory of the coupled KIM and underscores its potential for reliable extended range forecasting.

Looking forward, several challenges remain. The eastern Pacific warm bias in the coupled KIM should be rectified, potentially through improvements in the double ITCZ representation and associated convection–cloud–radiation feedbacks. In particular, this bias is also known to be closely linked to the underestimation of stratocumulus clouds in the eastern Pacific (Zhang et al., 2019), suggesting that improvements in low-cloud physical processes are required. Although ENSO skewness is more realistically simulated than in most models, El Niño intensity remains underestimated relative to observations, indicating the need for further refinement of nonlinear ocean–atmosphere coupling processes. Finally, given KIAPS's operational focus on extended-range prediction over East Asia, future work should place greater emphasis on evaluating and improving ENSO teleconnection impacts specifically in the East Asian region.

Code and data availability

The full source code of the Korean Integrated Model (KIM) is not publicly available due to institutional restrictions related to the development and maintenance of the operational numerical weather prediction system. Therefore, the full model code cannot be deposited in a public repository. The processed KIM simulation output and analysis scripts presented in this study will be made publicly available upon the reviewer's request. The ERA5 monthly averaged data on pressure levels and single levels were obtained from the Copernicus Climate Data Store under https://doi.org/10.24381/cds.6860a573 and https://doi.org/10.24381/cds.f17050d7, respectively (Hersbach et al., 2020). The ORAS5 global ocean reanalysis data were obtained from the Copernicus Climate Data Store under https://doi.org/10.24381/cds.67e8eeb7 (Zuo et al., 2019). The NOAA Optimum Interpolation Sea Surface Temperature, version 2.1, is available under https://doi.org/10.25921/RE9P-PT57 (Huang et al., 2021). The Global Precipitation Climatology Project monthly precipitation data, version 2.3, are available under https://doi.org/10.7289/V56971M6 (Adler et al., 2018). The NCEP–DOE Reanalysis 2 data are available under https://doi.org/10.5065/KVQZ-YJ93 (Kalnay et al., 2018). The CMIP6 model output used in this study was obtained through the Earth System Grid Federation (ESGF) and is freely obtained via the ESGF data portals after registration (https://aims2.llnl.gov/search). The exact model and experiment data sets, including their persistent CMIP6 DataCite DOIs, are cited individually in the in Table 1.

Author contributions

M.-S. Koo designed and carried out the experiments. S.-R. Yeo performed the analysis, organized the scientific content, and prepared the manuscript. M.-S. Koo, E. Lee and K.-H. Seol contributed to the discussion and interpretation of the results. All authors reviewed and approved the final version of the manuscript.

Competing interests

The authors declare that they have no competing interests.

Financial support

This work was supported by the R&D project "Development of a Next Generation Numerical Weather Prediction Model by the Korea Institute of Atmospheric Prediction System (KIAPS)", funded by the Korea Meteorological Administration (Grant No. KMA2020-02212).

https://doi.org/10.5194/egusphere-2026-4120
Preprint. Discussion started: 7 August 2026

Review statement

References

Adler, R. F., Sapiano, M. R., Huffman, G. J., Wang, J., Gu, G., Bolvin, D. T., ... Shin, D. B.: The global precipitation climatology project (GPCP) monthly analysis (new version 2.3) and a review of 2017 global precipitation, Atmosphere, https://doi.org/10.3390/atmos9040138, 2018.

Alexander, M. A., Bladé, I., Newman, M., Lanzante, J. R., Lau, N. C., and Scott, J. D.: The atmospheric bridge: the influence of ENSO teleconnections on air-sea interaction over the global oceans, J. Climate, https://doi.org/10.1175/1520-0442(2002)015%3c2205:TABTIO%3e2.0.CO;2, 2002.

An, S. I. and Jin, F. F.: Collective role of thermocline and zonal advective feedbacks in the ENSO mode, J. Climate, https://doi.org/10.1175/1520-0442(2001)014<3421:CROTTA>2.0.CO;2, 2001.

An, S. I. and Jin, F. F.: Nonlinearity and asymmetry of ENSO, J. Climate, https://doi.org/10.1175/1520-0442(2004)017,2399:NAAOE.2.0.CO;2, 2004.

Baek, S. and Kim, J.: Subgrid-scale topographic effects on radiation for global weather forecast models, Atmosphere, https://doi.org/10.3390/atmos15040479, 2024.

Chen, H. C. and Jin, F. F.: Simulations of ENSO phase-locking in CMIP5 and CMIP6, J. Climate, https://doi.org/10.1175/JCLI-D-20-0774.1, 2021.

Choi, S. J. and Hong, S. Y.: A global non-hydrostatic dynamical core using the spectral element method on a cubed-sphere grid, Asia-Pac. J. Atmos. Sci., https://doi.org/10.1007/s13143-016-0005-0, 2016.

Collins, M., et al.: The impact of global warming on the tropical Pacific Ocean and El Niño, Nat. Geosci., https://doi.org/10.1038/ngeo868, 2010.

Durack, P. J., et al.: The Coupled Model Intercomparison Project (CMIP): Reviewing project history, evolution, infrastructure and implementation, EGUsphere, https://doi.org/10.5194/egusphere-2024-3435, 2025.

Ek, M. B., Mitchell, K. E., Lin, Y., Rogers, E., Grunmann, P., Koren, V., et al.: Implementation of Noah land surface model advances in the National Centers for Environmental Prediction operational mesoscale Eta model, J. Geophys. Res., https://doi.org/10.1029/2002JD003296, 2003.

Eyring, V., Bony, S., Meehl, G. A., Senior, C. A., Stevens, B., Stouffer, R. J., and Taylor, K. E.: Overview of the Coupled Model Intercomparison Project Phase 6 (CMIP6) experimental design and organization, Geosci. Model Dev., https://doi.org/10.5194/gmd-9-1937-2016, 2016.

Griffies, S. M., Biastoch, A., Böning, C., Bryan, F., Danabasoglu, G., Chassignet, E. P., ... Yin, J.: Coordinated ocean-ice reference experiments (COREs), Ocean Model., https://doi.org/10.1016/j.ocemod.2008.08.007, 2009.

Guilyardi, E.: El Niño–mean state–seasonal cycle interactions in a multi-model ensemble, Clim. Dynam., https://doi.org/10.1007/s00382-005-0084-6, 2006.

https://doi.org/10.5194/egusphere-2026-4120
Preprint. Discussion started: 7 August 2026

Guilyardi, E., Wittenberg, A., Fedorov, A., Collins, M., Wang, C., Capotondi, A., ... Stockdale, T.: Understanding El Niño in ocean–atmosphere general circulation models: Progress and challenges, Bull. Amer. Meteorol. Soc., https://doi.org/10.1175/2008BAMS2387.1, 2009.

Han, J. Y.: Impact of different scale-aware cumulus parameterizations on precipitation forecasts over Korea, Atmos. Res., https://doi.org/10.1016/j.atmosres.2024.107990, 2025.

Hersbach, H., Bell, B., Berrisford, P., Hirahara, S., Horányi, A., Muñoz-Sabater, J., ... et al.: The ERA5 global reanalysis, Q. J. Roy. Meteor. Soc., https://doi.org/10.1002/qj.3803, 2020.

Hong, S. Y., Kwon, Y. C., Kim, T. H., Kim, J. E., Choi, S. J., Kwon, I. H., ... Kim, D. I.: The Korean Integrated Model (KIM) system for global weather forecasting, Asia-Pac. J. Atmos. Sci., https://doi.org/10.1007/s13143-018-0028-y, 2018.

Huang, B., Liu, C., Banzon, V., Freeman, E., Graham, G., Hankins, B., ... Zhang, H. M.: Improvements of the daily optimum interpolation sea surface temperature (DOISST) version 2.1, J. Climate, https://doi.org/10.1175/JCLI-D-20-0166.1, 2021.

Jiang, W., Huang, P., Huang, G., and Ying, J.: Origins of the excessive westward extension of ENSO SST simulated in CMIP5 and CMIP6 models, J. Climate, https://doi.org/10.1175/JCLI-D-20-0551.1, 2021.

Kalnay, E., Kanamitsu, M., Kistler, R., Collins, W., Deaven, D., Gandin, L., ... Joseph, D.: The NCEP/NCAR 40-year reanalysis project, Renewable Energy, https://doi.org/10.4324/9781315793245-15, 2018.

Kang, I. S. and Kug, J. S.: El Niño and La Niña sea surface temperature anomalies: Asymmetry characteristics associated with their wind stress anomalies, J. Geophys. Res., https://doi.org/10.1029/2001JD000393, 2002.

Kim, S. T. and Yu, J. Y.: The two types of ENSO in CMIP5 models, Geophys. Res. Lett., https://doi.org/10.1029/2012GL052006, 2012.

Kim, S. T., Cai, W., Jin, F. F., Santoso, A., Wu, L., Guilyardi, E., and An, S. I.: Response of El Niño sea surface temperature variability to greenhouse warming, Nat. Clim. Change, https://doi.org/10.1038/nclimate2326, 2014.

Kim, S. Y.: Effects of resolution-dependent excitation of parameterized frontal gravity waves on the middle atmosphere circulation in the Korean Integrated Model, J. Geophys. Res.-Atmos., https://doi.org/10.1029/2025JD044822, 2025.

Koo, M. S. and Hong, S. Y.: Refinement of mesoscale and turbulent-scale surface stresses in the Korean Integrated Model (KIM) for global weather forecasting, Wea. Forecasting, https://doi.org/10.1175/WAF-D-24-0012.1, 2025.

Koo, M. S., Lee, E., Cho, M. H., Gim, H. J., Han, Y. J., Park, J., ... Lee, E. H.: New Coupled Modeling System based on the Korean Integrated Model (KIM), Research activities in Earth System Modelling, WGNE Report No. 54, https://doi.org/10.5281/zenodo.14753296, 2025.

Kwak, K., Song, H., Yeo, N., Chang, E. C., Koo, M. S., Lee, E., and Park, J.: Improved subseasonal prediction of atmospheric energy transport over the Northwest Pacific using an atmosphere–ocean coupled model, Mon. Wea. Rev., https://doi.org/10.1175/MWR-D-24-0158.1, 2025.

Lee, E. H., Cho, S., Cho, K. H., Han, J. Y., Lee, Y., and Kim, J.: Forecast accuracy and physics sensitivity in high-resolution simulations of precipitation events in summer 2022 by the Korean Integrated Model, Asia-Pac. J. Atmos. Sci., https://doi.org/10.1007/s13143-024-00358-4, 2024.

https://doi.org/10.5194/egusphere-2026-4120
Preprint. Discussion started: 7 August 2026

Larson, J., Jacob, R., and Ong, E.: The model coupling toolkit: A new Fortran90 toolkit for building multiphysics parallel coupled models, Int. J. High Perform. C., https://doi.org/10.1177/1094342005056115, 2005.

Liu, B., Gan, B., Cai, W., Wu, L., Geng, T., Wang, H., ... Jia, F.: Will increasing climate model resolution be beneficial for ENSO simulation?, Geophys. Res. Lett., https://doi.org/10.1029/2021GL096932, 2022.

Madec, G. and the NEMO System Team: NEMO Ocean Engine Reference Manual, Zenodo, https://doi.org/10.5281/zenodo.1464816, 2024.

Martineau, P., Nakamura, H., and Kosaka, Y.: Influence of ENSO on North American subseasonal surface air temperature variability, Weather Clim. Dynam., https://doi.org/10.5194/wcd-2-395-2021, 2021.

Neelin, J. D., Jin, F. F., and Syu, H. H.: Variations in ENSO phase locking, J. Climate, https://doi.org/10.1175/1520-0442(2000)013<2570:VIEPL>2.0.CO;2, 2000.

Niu, G. Y., Yang, Z. L., Mitchell, K. E., Chen, F., Ek, M. B., Barlage, M., et al.: The community Noah land surface model with multiparameterization options (Noah-MP): 1. Model description and evaluation with local-scale measurements, J. Geophys. Res., https://doi.org/10.1029/2010JD015139, 2011.

Park, J. H., Sung, H. J., Koo, M. S., Park, J., Park, R. S., Han, K. H., ... Kim, B. M.: Impact of Arctic sea ice representation on extended medium-range forecasting: A case study of the 2016 Barents-Kara Sea warming event, Asia-Pac. J. Atmos. Sci., https://doi.org/10.1007/s13143-024-00392-2, 2025.

Planton, Y. Y., Guilyardi, E., Wittenberg, A. T., Lee, J., Gleckler, P. J., Bayr, T., ... Voldoire, A.: Evaluating climate models with the CLIVAR 2020 ENSO metrics package, Bull. Amer. Meteorol. Soc., https://doi.org/10.1175/BAMS-D-19-0337.1, 2021.

Zhang, T. and Sun, D. Z.: ENSO asymmetry in CMIP5 models, J. Climate, https://doi.org/10.1175/JCLI-D-13-00454.1, 2014.

WAVEWATCH III Development Group: User manual and system documentation of WAVEWATCH III® version 6.07, NOAA/NWS/NCEP/MMAB Technical Note 333, https://doi.org/10.25923/f0rt-7711, 2019.

Wallace, J. M. and Gutzler, D. S.: Teleconnections in the geopotential height field during the Northern Hemisphere winter, Mon. Wea. Rev., https://doi.org/10.1175/1520-0493(1981)109<0784:TITGHF>2.0.CO;2, 1981.

Vancoppenolle, M., Rousset, C., Blockley, E., and the NEMO Sea Ice Working Group: SI3 – Sea Ice modelling Integrated Initiative – The NEMO Sea Ice Engine, Zenodo, https://doi.org/10.5281/zenodo.7534900, 2023.

Vitart, F., Balmaseda, M. A., Ferranti, L., and Anderson, D.: Westerly wind events and the 1997/98 El Niño event in the ECMWF seasonal forecasting system: A case study, J. Climate, https://doi.org/10.1175/1520-0442(2003)016<3153:WWEATE>2.0.CO;2, 2003.

Wengel, C., Lee, S. S., Stuecker, M. F., Timmermann, A., Chu, J. E., and Schloesser, F.: Future high-resolution El Niño/Southern Oscillation dynamics, Nat. Clim. Change, https://doi.org/10.1038/s41558-021-01132-4, 2021.

Yeo, S. R., Lee, E. H., and Jun, S. Y.: Evaluation of climate variability and its impacts over East Asia in AMIP-type simulation of the Korean Integrated Model, Adv. Atmos. Sci., https://doi.org/10.1007/s00376-026-5563-1, 2026.

https://doi.org/10.5194/egusphere-2026-4120
Preprint. Discussion started: 7 August 2026

Zuo, H., Balmaseda, M. A., Tietsche, S., Mogensen, K., and Mayer, M.: The ECMWF operational ensemble reanalysis–analysis system for ocean and sea ice: A description of the system and assessment, Ocean Sci., https://doi.org/10.5194/os-15-779-2019, 2019.

Zhang, J. and Rothrock, D. A.: Modeling global sea ice with a thickness and enthalpy distribution model in generalized curvilinear coordinates, Mon. Wea. Rev., https://doi.org/10.1175/1520-0493(2003)131<0845:MGSIWA>2.0.CO;2, 2003.

Zhang, G. J., Song, X., and Wang, Y.: The double ITCZ syndrome in GCMs: A coupled feedback problem among convection, clouds, atmospheric and ocean circulations, Atmos. Res., https://doi.org/10.1016/j.atmosres.2019.06.023, 2019.

Zhao, Y. and Sun, D. Z.: ENSO asymmetry in CMIP6 models, J. Climate, https://doi.org/10.1175/JCLI-D-21-0975.1, 2022.